Title

Vulnerability to APOBEC3G linked to the pathogenicity of deltaretroviruses.

Journal

Proceedings of the National Academy of Sciences, 121(13)

Authors

Shichijo, Takafumi
Yasunaga, Jun-Ichirou
Sato, Kei
et al.

Publication Date

2024-03-26

DOI

10.1073/pnas.2309925121

Peer reviewed

PNAS RESEARCH ARTICLE | MICROBIOLOGY OPEN ACCESS

Vulnerability to APOBEC3G linked to the pathogenicity of deltaretroviruses

Takafumi Shichijo[a,b], Jun-ichirou Yasunaga[a,b,1], Kei Sato[c,d], Kisato Nosaka[a], Kosuke Toyoda[a,b], Miho Watanabe[a], Wenyi Zhang[a], Yoshio Koyanagi[e], Edward L. Murphy[f,g,h], Roberta L. Bruhn[h], Ki-Ryang Koh[i], Hirofumi Akari[j], Terumasa Ikeda[k,l,m], Reuben S. Harris[l,m], Patrick L. Green[n,o], and Masao Matsuoka[a,b,1]

Edited by Robert Gallo, University of Maryland School of Medicine, Baltimore, MD; received June 13, 2023; accepted January 29, 2024

Human retroviruses are derived from simian ones through cross-species transmission. These retroviruses are associated with little pathogenicity in their natural hosts, but in humans, HIV causes AIDS, and human T-cell leukemia virus type 1 (HTLV-1) induces adult T-cell leukemia–lymphoma (ATL). We analyzed the proviral sequences of HTLV-1, HTLV-2, and simian T-cell leukemia virus type 1 (STLV-1) from Japanese macaques (*Macaca fuscata*) and found that APOBEC3G (A3G) frequently generates G-to-A mutations in the HTLV-1 provirus, whereas such mutations are rare in the HTLV-2 and STLV-1 proviruses. Therefore, we investigated the mechanism of how HTLV-2 is resistant to human A3G (hA3G). HTLV-1, HTLV-2, and STLV-1 encode the so-called antisense proteins, HTLV-1 bZIP factor (HBZ), Antisense protein of HTLV-2 (APH-2), and STLV-1 bZIP factor (SBZ), respectively. APH-2 efficiently inhibits the deaminase activity of both hA3G and simian A3G (sA3G). HBZ and SBZ strongly suppress sA3G activity but only weakly inhibit hA3G, suggesting that HTLV-1 is incompletely adapted to humans. Unexpectedly, hA3G augments the activation of the transforming growth factor (TGF)-β/Smad pathway by HBZ, and this activation is associated with ATL cell proliferation by up-regulating *BATF3/IRF4* and *MYC*. In contrast, the combination of APH-2 and hA3G, or the combination of SBZ and sA3G, does not enhance the TGF-β/Smad pathway. Thus, HTLV-1 is vulnerable to hA3G but utilizes it to promote the proliferation of infected cells via the activation of the TGF-β/Smad pathway. Antisense factors in each virus, differently adapted to control host cellular functions through A3G, seem to dictate the pathogenesis.

deltaretrovirus | HTLV-1 | APOBEC3G | HBZ | TGF-β

Significance

Cross-species transmission of viruses is frequently linked to increased pathogenicity. HIV-1 causes AIDS in humans, while SIV-1 is not as pathogenic in its natural hosts. Human T-cell leukemia virus type 1 (HTLV-1) causes adult T-cell leukemia–lymphoma (ATL), whereas its related retrovirus, human T cell leukemia virus type 2, shows little pathogenicity in humans. The mechanism by which HTLV-1 is so pathogenic in its new host remains unknown. This study shows that HTLV-1 is inadequately adapted to the human antiretroviral factor, APOBEC3G, but utilizes it to promote proliferation of HTLV-1-infected and ATL cells, resulting in its pathogenicity. We reveal one of the mechanisms by which HTLV-1, a deltaretrovirus, causes diseases in humans after cross-species transmission.

Human T-cell leukemia virus type 1 (HTLV-1) was the first human retrovirus to be found (1). Thereafter, HTLV-2, HIV type 1 (HIV-1), and HIV-2 were discovered (2–6). HTLV-1 induces several diseases in humans, including adult T-cell leukemia–lymphoma (ATL) and HTLV-1-associated myelopathy (HAM), whereas HIV-1 and HIV-2 cause acquired immunodeficiency syndrome (AIDS). Although both HTLV-1 and HIV target CD4 T cells in vivo, HIV decreases the number of CD4 T cells, while HTLV-1 increases it. Unlike these pathogenic human retroviruses, HTLV-2 shows limited to no pathogenicity in humans (7). Thus, pathogenicity is diverse among human retroviruses.

These human retroviruses originated from simian retroviruses. HTLV-1 is derived from simian T-cell leukemia virus type 1 (STLV-1), which entered into the human population by cross-species transmission approximately 20,000 to 50,000 y ago (8–10). Although HTLV-1 induces ATL in approximately 5% of infected individuals (11), development of T cell lymphomas was rarely reported in STLV-1-infected Japanese macaques (*Macaca fuscata*) (12), suggesting that the pathogenicity of STLV-1 is low in Japanese macaques. Furthermore, an outbreak of T cell lymphomas was reported in baboons and was likely caused by STLV-1 derived from the rhesus macaque (13). This strongly indicates that cross-species transmission is linked to increased pathogenicity of STLV-1. Likewise, simian immunodeficiency viruses are not very pathogenic in their natural hosts (14). SIVsmm, which naturally infects sooty mangabeys, is genetically close to HIV-2 (15, 16). SIVsmm shows a high pathogenicity for humans and rhesus macaques after cross-species transmission. Thus, cross-species transmission is closely associated with the pathogenicity of retroviruses. However, the mechanism(s) of precisely how cross-species transmission is linked to pathogenicity remains to be elucidated.

Cellular restriction factors for retroviruses inhibit viral replication and include APOBEC, Tetherin, and TRIM5α (17). APOBEC3G (A3G) functions as an innate defense mechanism against retroviruses by targeting single-stranded DNA (ssDNA) for mutation (via deamination) during reverse transcription, resulting in G-to-A mutations (18, 19). HIV counteracts

Author contributions: T.S., J.-i.Y., and M.M. designed research; T.S., J.i.Y., K.T., M.W., and W.Z. performed research; K.S., K.N., Y.K., E.L.M., R.L.B., K.-R.K., H.A., and P.L.G. contributed new reagents/analytic tools; T.S., J.-i.Y., K.T., and M.M. analyzed data; J.-i.Y., K.S., T.I., R.S.H., and M.M. supervision; and T.S., J.-i.Y., R.S.H., and M.M. wrote the paper.

The authors declare no competing interest.

This article is a PNAS Direct Submission.

[1]To whom correspondence may be addressed. Email: mamatsu@kumamoto-u.ac.jp or jyasunag@kumamoto-u.ac.jp.

This article contains supporting information online at https://www.pnas.org/lookup/suppl/doi:10.1073/pnas.2309925121/-/DCSupplemental.

Published March 19, 2024.

A3G through viral infectivity factor (Vif)-mediated degradation of A3G (20, 21). Thus, some retroviruses acquire resistance to A3G. The mechanism of resistance to A3G remains to be elucidated in deltaretroviruses (the genus of the *Retroviridae* family that includes HTLV-1 and its relatives). It has been reported that a peptide motif in the HTLV-1 nucleocapsid hinders human A3G (hA3G) packaging into the virions (22). However, G-to-A mutations by hA3G are frequently observed in the HTLV-1 proviruses of ATL cells (23, 24), indicating that HTLV-1 is not very resistant to hA3G.

In this study, we show that HTLV-1 is vulnerable to hA3G, whereas it is still resistant to simian A3G (sA3G). HTLV-1 bZIP factor (HBZ), a viral protein encoded by an antisense gene, binds to sA3G and inhibits its deaminase activity. The interaction of HBZ and hA3G fails to strongly inhibit deaminase activity, but interestingly and unexpectedly, these two proteins cooperate to enhance activation of the transforming growth factor (TGF-β)/Smad pathway, which promotes proliferation of HTLV-1-infected T cells and lymphomagenesis. In contrast, SBZ (STLV-1 bZIP) does not synergize with sA3G to enhance the activation of the TGF-β/Smad pathway. Thus, cross-species transmission has increased the pathogenicity of HTLV-1 in humans through the interactions of HBZ with the (normally antiretroviral) factor A3G.

Results

HTLV-1 Proviral Mutations in Infected individuals. We have reported that nonsense mutations are frequently detected in the proviruses of ATL patients (23). The sequence motifs of most nonsense mutations correspond to the target preference of A3G (23, 25). However, the frequencies of A3G-mediated mutations in HTLV-1 asymptomatic carriers (ACs), as well as in other deltaretroviral infections (HTLV-2 and STLV-1), have yet to be studied in detail. To investigate mutagenesis in vivo, we performed deep sequencing of full proviruses in 65 HTLV-1 ACs (Japanese subtype, n = 53; transcontinental subtype, n = 12), 18 HTLV-2-infected individuals (HTLV-2a, n = 11; HTLV-2b, n = 7), and 16 STLV-1-infected Japanese macaques (*SI Appendix,* Fig. S1 *A–D*). The data of proviral load were shown in *SI Appendix,* Table S1. The mutations observed in the proviral DNA sequences of the 65 HTLV-1 ACs are shown in Fig. 1*A*. Among 2,125 base substitutions detected in these HTLV-1 ACs, 73.0% of the mutations were G-to-A, and furthermore, 87.1 % of these G-to-A mutations were GG-to-AG, which corresponds to the preferred target sequence of hA3G (i.e., cDNA strand CC-to-CU deamination events) (Fig. 1*B*) (25). Most mutations detected in HTLV-1 ACs were confirmed to be GG-to-AG using HYPERMUT software (*SI Appendix,* Fig. S1*E*). The majority of these mutational events created premature stop codons (Fig. 1*C*). Notably, nonsense mutations in the *tax* gene were found in 97% (63 out of 65) of HTLV-1 carrier cases. The percentage of mutations in each sequence is variable among individuals from 0 to 27% as shown in Fig. 1*D* and SI Appendix Fig. S1 *F–H*. One of the nonsense mutations in *tax*, G7467A (W56*), was found in 58/65 HTLV-1 ACs (Fig. 1 *C* and *D* and *SI Appendix,* Fig. S1*F*). In comparison, nonsense mutations in the *HBZ* gene were detected rarely (Fig. 1*D* and *SI Appendix,* Fig. S1*H*). Since the *HBZ* gene is encoded by the minus strand of HTLV-1 provirus (26), G-to-A mutation in the minus strand does not generate stop codons.

Next, we investigated HTLV-2 proviruses, which are not etiologically associated with leukemia (7). Although HTLV-2 belongs to the same deltaretrovirus genus as HTLV-1 and encodes a similar regulatory gene (*tax2*), the frequency of G-to-A mutations in these proviruses (HTLV-2a and 2b) was much lower than analogous events in HTLV-1 (Fig. 1*E* for HTLV-2a and *SI Appendix,* Fig. S2*A* for HTLV-2b). Moreover, mutations in the target sequence preferred by hA3G comprised only 2.9% of total HTLV-2 mutations (Fig. 1*F*), indicating that HTLV-2 is resistant to hA3G compared with HTLV-1. Nonsense mutations were rarely detected in HTLV-2-infected individuals (16 out of 18 had no nonsense mutations) (Fig. 1*G* and *SI Appendix,* Fig. S2*B*). However, interestingly, in two independent cases, nonsense mutations in the *Antisense protein of HTLV-2* (*APH-2*) gene (Q87*) were associated with increased G-to-A mutations, suggesting that loss of APH-2 may increase viral susceptibility to A3G (*SI Appendix,* Fig. S2*C*). The *APH-2* gene is encoded in the minus strand of the HTLV-2 provirus (27).

Since STLV-1 is related to HTLV-1, we investigated the proviruses of STLV-1-infected Japanese macaques. We speculated that G-to-A mutations in the STLV-1 provirus would occur as frequently as in HTLV-1. Unexpectedly, we found that the rate of G-to-A mutations detected in STLV-1 was much lower than that of HTLV-1 (Fig. 1*H*). Furthermore, mutations of the target sequence preferred by A3G were only 7.4% of total STLV-1 mutations (Fig. 1*I*), indicating that STLV-1 is resistant to sA3G of Japanese macaques. Consistent with these findings, nonsense mutations were rarely observed in STLV-1 (Fig. 1*J*). These differences in the frequency of G-to-A mutations suggest that these deltaretroviruses have different susceptibilities to A3G.

Human A3G Generates G-to-A Mutations in the Provirus during De Novo Infection. Based on the results above, it is likely that hA3G induces the G-to-A mutations found in the HTLV-1 proviruses, and the less mutable HTLV-2 and STLV-1 proviruses are more resistant to hA3G/sA3G. To analyze the effect of hA3G on HTLV-1 proviral sequences in newly infected cells, we produced HTLV-1 viral particles (VPs) in hAPOBEC-overexpressing HEK293T cells and used these particles to infect Jurkat cells. The expression level of the different APOBECs in HEK293T cells was shown in *SI Appendix,* Fig. S2*D*. Sequencing of the proviruses in the newly infected Jurkat cells revealed many G-to-A mutations induced by hA3G, but not by hA3C/D/F/H (Fig. 1*K* and *SI Appendix,* Fig. S2*E*). Many of these G-to-A mutations corresponded to the identified mutated positions in HTLV-1 AC proviruses (*SI Appendix,* Fig. S2*F*). Frequencies of G-to-A mutations were much higher for in vitro experiments (Fig. 1*K*) compared with in vivo data (Fig. 1*A*), due to the fact that A3G is over-expressed. Further, mutant hA3G (hA3G-E259Q), which lacks deaminase activity, did not induce G-to-A mutations (*SI Appendix,* Fig. S2*G*), indicating that hA3G directly generates the G-to-A mutations in the HTLV-1 provirus. However, sA3G from Japanese macaques did not generate G-to-A mutations in the HTLV-1 provirus (Fig. 1*K*). Intriguingly, hA3G (also hA3C/D/F/H) did not induce G-to-A mutations in provirus of HTLV-2-infected Jurkat cells (Fig. 1*L* and *SI Appendix,* Fig. S2*E*). Further, hA3G, but not sA3G, induced G-to-A mutations in the provirus of STLV-1-infected cells (Fig. 1*M*). It is critical to show that the sA3G used in this study is functional. As shown in *SI Appendix,* Fig. S3*D*, sA3G suppressed infectivity of recombinant HIV, and this suppression was counteracted by HBZ or SBZ. Furthermore, the deaminase activity of sA3G was confirmed in experiments described in the following section (Fig. 2*A*). Taken together, these results show that both HBZ and SBZ are unable to inhibit hA3G in contrast to APH2. On the other hand, HBZ and SBZ can inhibit sA3G. Thus, the susceptibility of HTLV-1 and STLV-1 to human and sA3Gs appears to be similar, whereas HTLV-2 is resistant to hA3G.

Antisense Proteins Interact with A3G. As G-to-A mutations were detected rarely in HTLV-2/STLV-1 proviruses in vivo, we hypothesized that HTLV-2/STLV-1 have a mechanism(s)

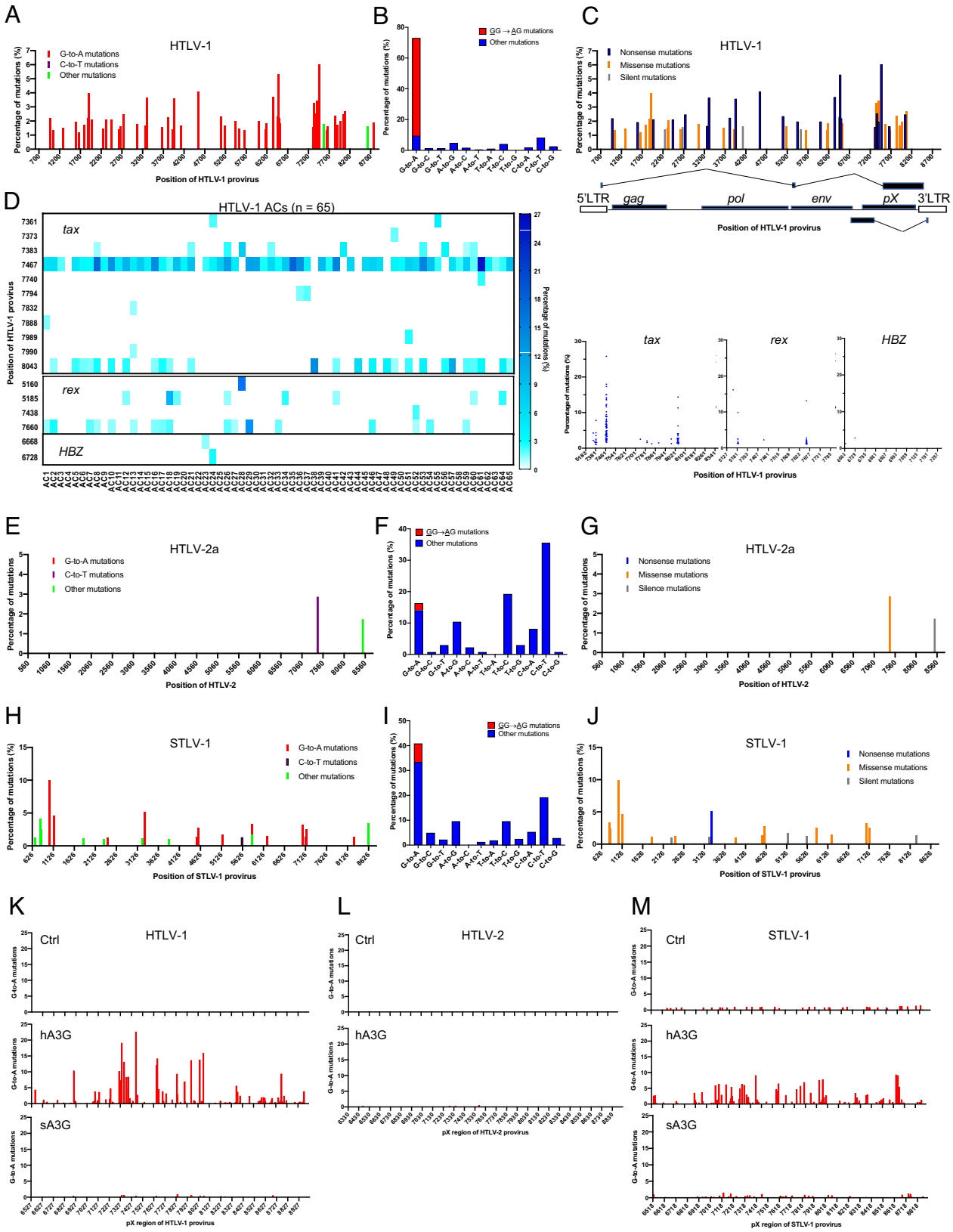

Fig. 1. A3G induces G-to-A mutations in HTLV-1, but not in HTLV-2 and STLV-1. (*A*) Frequency of mutations detected in the proviruses of 65 HTLV-1 ACs by deep sequencing. (*B*) These HTLV-1 mutations occurred primarily at human APOBEC3G (hA3G) preferred target sequences. (*C*) Frequency of nonsense mutations observed in 65 HTLV-1 ACs. (*D*) Heatmaps showing the frequency of nonsense mutations observed in the *tax, rex*, and *HBZ* genes in 65 HTLV-1 ACs. (*E*) Frequency of mutations detected in the proviruses of 11 HTLV-2a-infected individuals by deep sequencing. (*F*) These HTLV-2a mutations did not typically occur at hA3G preferred target sequences (GG→AG). (*G*) Frequency of nonsense mutations observed in 11 HTLV-2a-infected individuals. (*H*) Frequency of mutations detected in the proviruses of 16 STLV-1-infected Japanese macaques by deep sequencing. (*I*) Most of these STLV-1 mutations do not typically occur at sA3G target sequences. (*J*) Frequency of nonsense mutations observed in 16 STLV-1-infected Japanese macaques. Mutations detected in more than 10% of total cases are shown (*A* and *C* in HTLV-1 ACs, *E* and *G* in HTLV-2a-infected individuals, and *H* and *J* in STLV-1-infected Japanese macaques). (*K*) Frequency of G-to-A mutations detected in HTLV-1-infected cells expressing hA3G or sA3G in vitro. (*L*) Frequency of G-to-A mutations detected in HTLV-2-infected cells expressing hA3G in vitro. (*M*) Frequency of G-to-A mutations detected in STLV-1-infected cells expressing hA3G or sA3G in vitro. Experiments were performed twice (*K–M*).

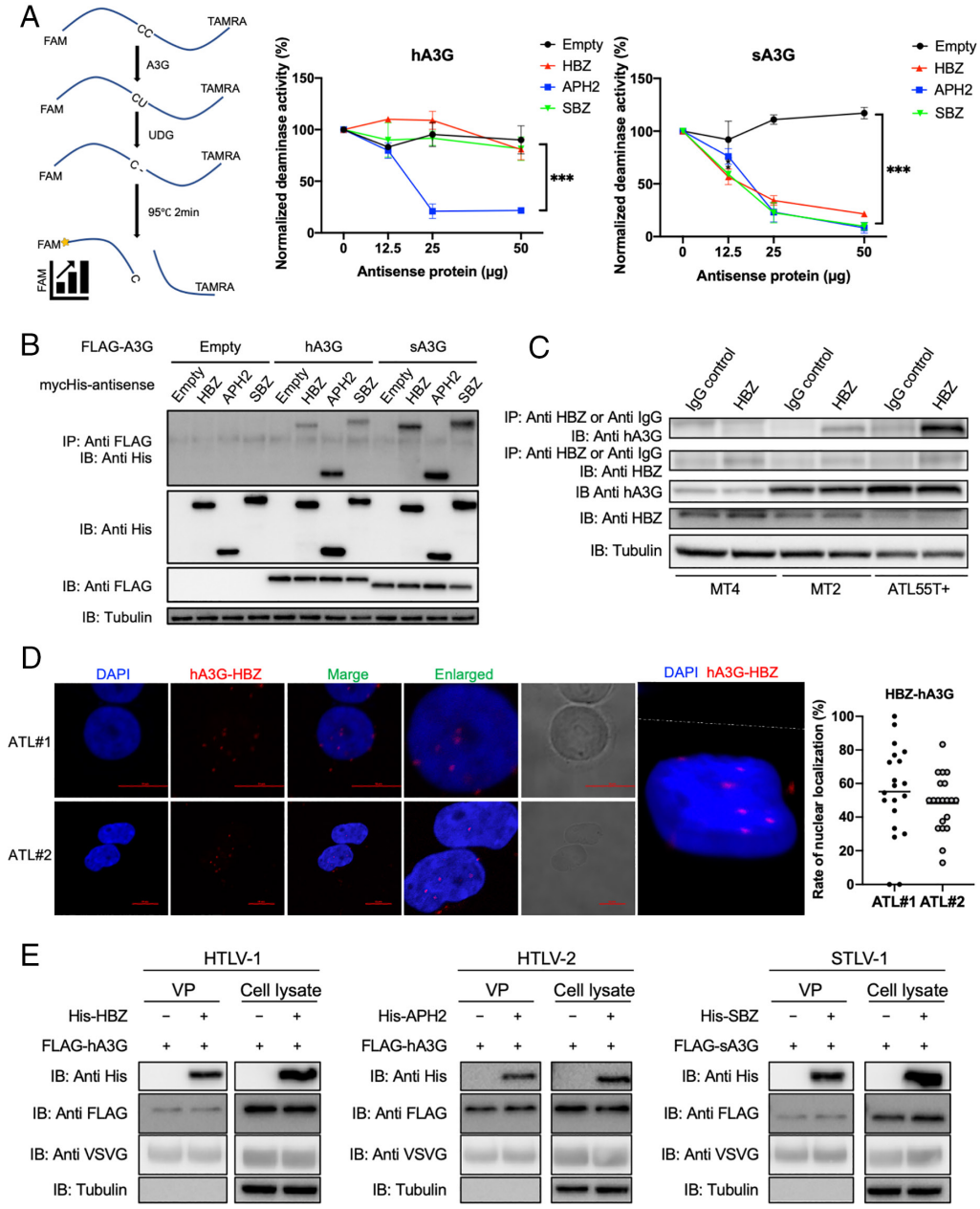

Fig. 2. Antisense proteins interact with A3G. (*A*) Schematic representation of the A3G-mediated deaminase activity assay (*Left*) and quantifications of A3G deaminase activity in the presence of increasing concentrations of HBZ, APH-2, and SBZ (normalized mean ± SD of triplicate experiments; one-way ANOVA with Tukey correction; ***$P < 0.001$) (*Right*). (*B*) Coimmunoprecipitation experiment showing the interaction between human or sA3G and the antisense proteins of HTLV-1, HTLV-2, and STLV-1 in transfected HEK293T cells. IP, immunoprecipitation; IB, immunoblot. (*C*) Coimmunoprecipitation experiment showing the interaction of endogenous hA3G with endogenous HBZ in HTLV-1-infected T cell lines (MT-2 and MT-4), and an ATL cell line (ATL-55T+). IP, immunoprecipitation; IB, immunoblot. (*D*) Complex of hA3G with HBZ in primary ATL cells (n = 2; ATL#1 and ATL#2) and 3-dimensional image of a fresh ATL cell (ATL#2) shown by confocal z-stacking, detected by the Duolink Proximity Ligation Assay (*Left*) and rate of nuclear localization of HBZ-hA3G complex (*Right*). (*E*) Immunoblot showing the incorporation of both A3G and antisense proteins into HTLV-1, HTLV-2, and STLV-1 VP. All experiments were performed at least twice.

to counteract hA3G/sA3G, perhaps functionally analogous to HIV-1/SIV Vif protein, which facilitates degradation of h/sA3G (20, 21). To investigate the mechanism by which HTLV-2 counteracts hA3G, we used a single-cycle infectious assay of HIV-1. Among the accessory and regulatory genes of HTLV-2, we found that the antisense protein APH-2 inhibited the hA3G-mediated suppression of HIV infectivity (*SI Appendix,* Fig. S3 *A–C*). In contrast, neither *HBZ* nor *SBZ* (the antisense genes in HTLV-1 and STLV-1, respectively) recovered HIV infectivity in the presence of hA3G, and they each recovered HIV infectivity weakly in the presence of sA3G (*SI Appendix,* Fig. S3*D*) (12, 26).

Next, we analyzed whether the antisense proteins, HBZ, APH-2, and SBZ, possess anti-A3G activity using an in vitro ssDNA deamination assay (Fig. 2*A* and *SI Appendix,* Fig. S3*E*) (28). APH-2 inhibited the deaminase activity of both human and sA3G (Fig. 2*A*). Neither HBZ nor SBZ influenced the deaminase activity of hA3G, whereas they each strongly inhibited that of sA3G (Fig. 2*A*). These results are consistent with the above findings that overexpressed hA3G induces G-to-A mutations in HTLV-1 and STLV-1 but not in HTLV-2, while sA3G does not induce them in either HTLV-1 or STLV-1 (Fig. 1 *K–M*).

To investigate the molecular mechanism by which these antisense proteins, when matched with the appropriate (human or simian) A3G, inhibit A3G activity, we first evaluated the degradation of A3G in the presence of antisense proteins. Unlike Vif, these antisense proteins did not degrade A3G (*SI Appendix,* Fig. S4*A*). To further study the mechanism of A3G inhibition, we next performed coimmunoprecipitation experiments. All three antisense proteins bound to both hA3G and sA3G (Fig. 2*B*). The binding of APH-2 to hA3G appears to be more intense compared to that of HBZ and SBZ (Fig. 2*B*), and the interaction of HBZ/SBZ with sA3G was stronger compared to that with hA3G (Fig. 2*B*). Furthermore, an endogenous interaction between hA3G with HBZ could be confirmed (Fig. 2*C*). For this experiment, we chose T cell lines with higher A3G expression (MT-2, MT-4 and ATL55T+) (*SI Appendix,* Fig. S4*B*). The expression level of *HBZ* mRNA was shown in *SI Appendix,* Fig. S4*B*. The interaction between hA3G and HBZ was also observed in primary ATL cells of

two cases using Duolink proximity ligation assay (PLA) (Fig. 2*D*) (29). Coimmunoprecipitation experiments using deletion mutants showed that the N-terminal domain of hA3G/sA3G interacts with HBZ, SBZ or APH-2 (*SI Appendix,* Fig. S4 *C–E*). The central domains of HBZ and SBZ were responsible for binding to hA3G and sA3G, whereas the nonconventional basic leucine zipper domain of APH-2 bound to both A3Gs (*SI Appendix,* Fig. S4 *F–I*).

Vif inhibits incorporation of A3G into the HIV virion through enhanced degradation of A3G protein (18). Therefore, we assessed the incorporation of A3G and antisense proteins into VP. As shown in Fig. 2*E*, both A3G and antisense proteins were incorporated into HTLV-1, HTLV-2, and STLV-1 virus particles. Further, the incorporation of both endogenous hA3G and HBZ into HTLV-1 VP was confirmed in MT-2 cells (*SI Appendix,* Fig. S4*J*). Unlike for HIV-1, these antisense viral proteins do not promote the degradation of A3G but bind to it and somehow impede its deaminase activity.

HBZ and hA3G Activate the TGF-β/Smad Signaling Pathway. As shown above, HBZ, like SBZ, can bind to and inhibit sA3G, while it does not inhibit hA3G despite binding to it. Meanwhile, APH-2 strongly binds and hinders hA3G. We hypothesize that the inability of HBZ to inhibit hA3G reflects the inadequate adaptation of HTLV-1 to humans. Intriguingly, expression of *hA3G* in ATL cells in aggressive types of ATL (acute and lymphoma-type) is higher than that in healthy donor cells (Fig. 3*A*), suggesting that hA3G may somehow be associated with leukemogenesis. However, despite the high expression level of hA3G in ATL patients and the fact that HBZ does not inhibit its deaminase activity, the APOBEC-related signature is not dominant in single-nucleotide variants by whole genome sequencing in ATL cells (30), indicating that hA3G does not cause somatic mutations in ATL cells. This makes sense because A3G is a cellular restriction factor that targets ssDNA of retroviruses. If hA3G is associated with leukemogenesis in ATL cells, it is by some other mechanism(s).

To explore how hA3G might contribute to ATL leukemogenesis, we performed RNA sequencing (RNA-seq) in hA3G knockdown ATL cells. Gene set enrichment analysis (GSEA) showed that TGF-β/Smad signaling pathway–associated gene sets are altered in the hA3G knockdown ATL cells (Fig. 3*B*). Consistent with this finding, a luciferase assay using a TGF-β responsive reporter (3TP-Lux) showed that hA3G activates the TGF-β/Smad pathway, whereas its activation by sA3G was marginal (Fig. 3*C*). We have reported that HBZ activates the TGF-β/Smad pathway through interaction with Smads and p300 (31). Importantly, HBZ synergistically enhances TGF-β/Smad signaling activated by hA3G, whereas SBZ (with sA3G) and APH-2 (with hA3G) did not have such an effect (Fig. 3*D* and *SI Appendix,* Fig. S5 *A–C*). Additionally, the activation of TGF-β/Smad signaling by HBZ was suppressed in hA3G knockdown HepG2 cells (*SI Appendix,* Fig. S5*D*). Thus, HBZ and hA3G cooperate to activate the TGF-β/Smad signaling pathway in a way that SBZ and sA3G do not.

To elucidate which region of hA3G is critical for this activation, we generated deletion mutants and found that the N-terminal region is critical for activation of the TGF-β/Smad pathway (*SI Appendix,* Fig. S5*E*). In particular, the 12 to 17th amino acids are indispensable (Fig. 3*E*). Alanine scanning mutagenesis of this region identified the 17th residue (phenylalanine) as being most important for the activation (Fig. 3*F*). Furthermore, the F17A mutant of hA3G did not enhance activation of TGF-β/Smad signaling by HBZ (*SI Appendix,* Fig. S5*F*).

A3G and HBZ Interact with Smad2/3. To study how HBZ and A3G activate the TGF-β/Smad pathway, we first performed coimmunoprecipitation experiments to check for interaction between hA3G and Smad. As shown in *SI Appendix,* Fig. S6*A*, hA3G interacts with Smad2/3/4/7 in cotransfected HepG2 cells. We then tested whether the endogenous proteins also interact. We found that endogenous hA3G interacts with Smad2/3, but not with Smad7, in human T cell lines (Fig. 4*A* and *SI Appendix,* Fig. S6*B*), suggesting that hA3G enhances TGF-β/Smad signaling via interaction with Smad2/3. The level of *Smad3* mRNA transcripts was higher in aggressive ATL patients than in healthy donors, while *Smad2* and *Smad7* transcripts were not up-regulated (Fig. 4*B*). To analyze the interaction between hA3G and Smad3, colocalization of hA3G with Smad3 was evaluated by immunofluorescence analysis and Duolink PLA. As shown in Fig. 4*C*, TGF-β treatment resulted in the relocalization of hA3G from the cytoplasm to the nuclear compartment via interaction with Smad3 in Hela cells. Furthermore, in the presence of TGF-β, the hA3G-Smad3 complex was detected in the nucleus by Duolink PLA in primary ATL cells (Fig. 4*D*).

In hA3G knockdown ATL cells, the gene set of protein tyrosine kinase activity was down-regulated as determined by GSEA (*SI Appendix,* Fig. S6*C*). Since the phosphorylation of Smad2/3 is necessary to activate the TGF-β/Smad signaling pathway, Smad2/3 phosphorylation was evaluated in cells expressing various levels of hA3G. As shown in Fig. 4*E* and *SI Appendix,* Fig. S6*D*, hA3G enhanced the phosphorylation of Smad3, but not Smad2, in a dose-dependent manner. We have reported that HBZ activates TGF-β/Smad signaling through its interaction with Smad2/3 and p300 (31). However, suppressed expression of hA3G did not influence the binding between HBZ and Smad3, and HBZ did not phosphorylate either Smad2 or Smad3 (Fig. 4*F* and *SI Appendix,* Fig. S6 *E* and *F*), indicating that hA3G enhances TGF-β/Smad signaling by a mechanism(s) differing from that of HBZ. The detailed mechanism(s) how A3G increase the phosphorylation of Smad3 remains to be elucidated. Taken together, our results suggest that HBZ and A3G function cooperatively on this pathway.

Inhibition of the TGF-β/Smad Signaling Pathway Suppresses the Proliferation of ATL Cells. Having shown that both HBZ and hA3G activate the TGF-β/Smad signaling pathway, we still needed to see whether activation of this pathway is associated with the leukemogenesis of ATL. The TGF-β/Smad signaling pathway is generally known as a suppressor of T cell growth, not a promoter of it. To investigate this matter, we performed cell proliferation assays in HTLV-1-infected and noninfected T cell lines using SB431542, an inhibitor of the TGF-β type I receptor, or SIS3-HCl, an inhibitor of Smad3 phosphorylation. As shown in Fig. 5*A* and *SI Appendix,* Fig. S7*A*, blockage of the TGF-β receptor suppressed cell growth in HTLV-1-infected and ATL cell lines in a dose-dependent manner, whereas it slightly activated cell growth in several noninfected T cell lines (Fig. 5*B* and *SI Appendix,* Fig. S7*B*). Similarly, SIS3-HCl suppressed cell growth, especially in HTLV-1-infected and ATL cells (Fig. 5 *C* and *D* and *SI Appendix,* Fig. S7 *C* and *D*). The effects of these inhibitors were variable among ATL cell lines. TL-Om1 and ATL-43Tb(-) were relatively resistant to these inhibitors (*SI Appendix,* Fig. S7 *A* and *C*). Furthermore, the suppressive effects by these inhibitors were partial, suggesting that the TGF-β/Smad pathway is responsible for a part of the proliferative process. These results indicate that activation of TGF-β/Smad signaling promotes the proliferation of ATL cells, even though for uninfected T cells it is generally known as suppressor of growth.

To further understand the mechanism by which the blocking of TGF-β/Smad signaling inhibits ATL cell growth, we performed RNA-seq in ATL cell lines treated with or without SB431542. GSEA showed that cell cycle, G2M, and E2F gene sets were down-regulated and that of p53 was up-regulated in the SB431542-treated group

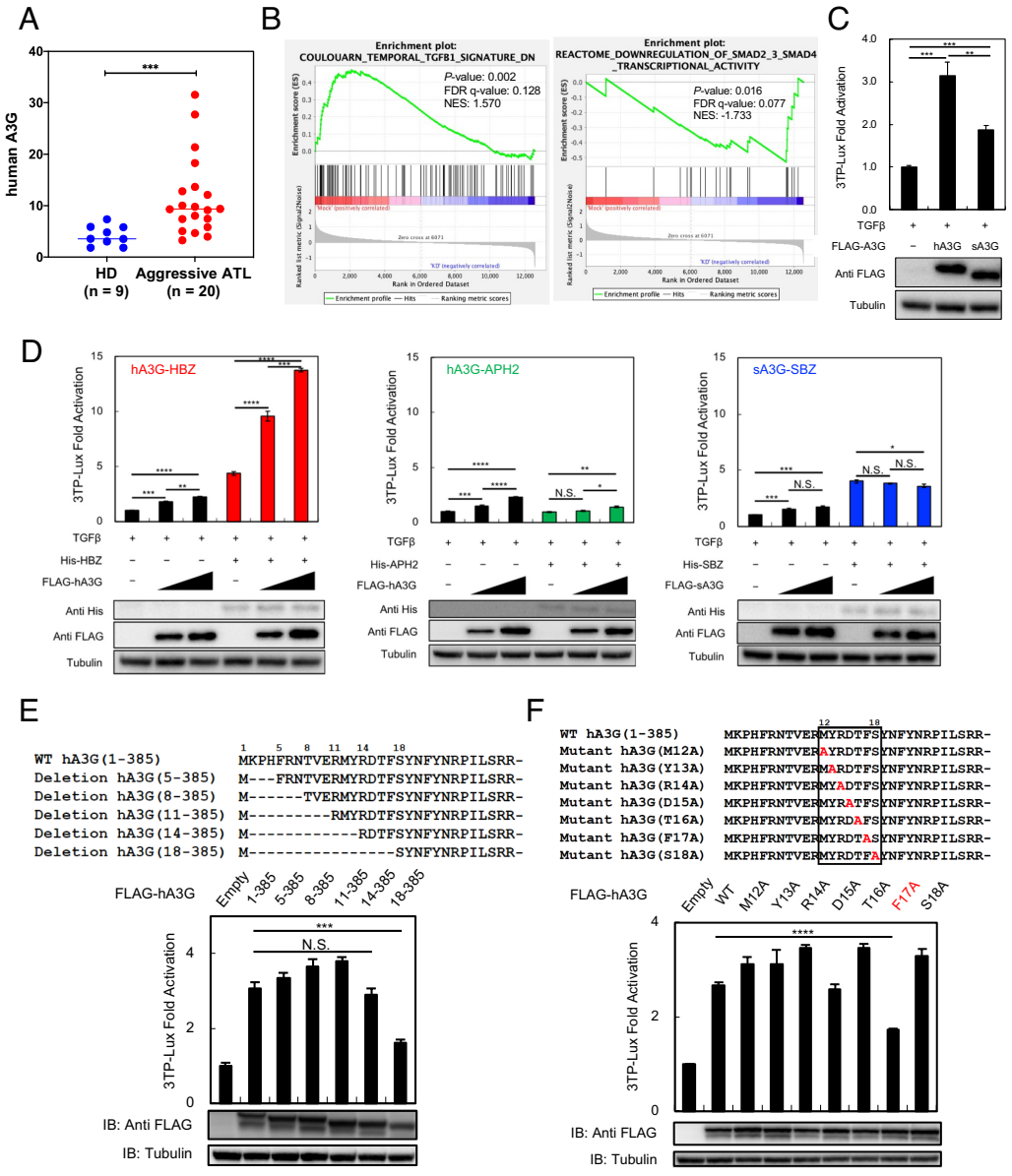

Fig. 3. hA3G cooperates with HBZ to activate the TGF-β/SMAD pathway. (*A*) Expression of hA3G in healthy donors (n = 9) and patients with aggressive ATL (acute, and lymphoma type ATL) (n = 20) by RT-qPCR (triplicate experiments; one-way ANOVA with Tukey correction; ***$P < 0.001$). (*B*) Gene signatures that are significantly enriched in hA3G-knockdown ATL cells (ATL-55T+), based on GSEA analysis with RNA-seq. (*C*) Luciferase activity of 3TP-Lux under the control of a TGF-β responsive element in cells expressing hA3G or sA3G (normalized mean ± SD of triplicate experiments; two-tailed unpaired Student's *t* test; **$P < 0.01$; ***$P < 0.001$). (*D*) Luciferase activity of 3TP-Lux under the control of a TGF-β responsive element in cells coexpressing HBZ with hA3G (*Left*), APH-2 with hA3G (*Middle*), or SBZ with sA3G (*Right*) (normalized mean ± SD of triplicate experiments; two-tailed unpaired Student's *t* test; *$P < 0.05$; **$P < 0.01$; ***$P < 0.001$; ****$P < 0.0001$). (*E*) Luciferase activity of 3TP-Lux under the control of a TGF-β responsive element in cells expressing deletion mutants of the N-terminal region of hA3G (normalized mean ± SD of triplicate experiments; two-tailed unpaired Student's *t* test; ***$P < 0.001$). IB, immunoblot. (*F*) Luciferase activity of 3TP-Lux under the control of a TGF-β responsive element in cells expressing alanine scanning mutants of the 12 to 18th amino acids of hA3G (normalized mean ± SD of triplicate experiments; two-tailed unpaired Student's *t* test; ****$P < 0.0001$). IB, immunoblot.

(*SI Appendix*, Fig. S8*A*). Of note, the *MYC*-associated gene sets were the most down-regulated in the SB431542-treated group (Fig. 5 *E* and *F*). Further, *c-Myc* expression was down-regulated in SIS3-HCl-treated ATL cells, but up-regulated in treated Hut78 cells, which are uninfected with HTLV-1 (*SI Appendix*, Fig. S8*B*). Stimulation of TGF-β/Smad signaling promoted *c-Myc* expression in ATL cells (*SI Appendix*, Fig. S8*C*). In most cells, *MYC* expression is generally inhibited by the TGF-β/Smad signaling, not promoted by it; thus, this discrepancy might be a clue as to why ATL cells differ in their response to TGF-β/Smad signaling.

BATF3 and IRF4 have been reported to be associated with the proliferation of ATL cells through upregulation of the *MYC* gene (32). We found that the expression of *BATF3* and *IRF4* was suppressed by inhibition of TGF-β/Smad signaling and promoted by stimulation of TGF-β/Smad signaling in ATL cell lines (Fig. 5*G* and *SI Appendix*, Fig. S9 *A–D*). Multiplex mass-cytometry (CyToF) indicated that TGF-β expression was indeed correlated with BATF3 and IRF4 in primary ATL cells (Fig. 5*H*). Furthermore, chromatin immunoprecipitation (ChIP) sequencing analysis shows that phosphorylated Smad3 is enriched at the transcriptional start site of *BATF3* and *IRF4* (Fig. 5 *I* and *J*). These results suggest that TGF-β/Smad signaling, activated by hA3G and HBZ, promotes ATL cell proliferation via the activation of *BATF3/IRF4* and *MYC*.

Finally, we evaluated tumor growth using a mouse xenograft model (Fig. 6*A*). As expected, tumor growth was significantly suppressed in both the SB431542- and SIS3-HCl-treated groups (Fig. 6 *B–D*), suggesting that TGF-β/Smad signaling is crucial for in vivo ATL tumor growth.

Discussion

Human retroviruses originate from simian ones. Importantly, SIV, with the exception of SIVcpz, is not pathogenic for its natural host (14, 16). However, HIV-1 causes the serious disease AIDS in humans. It remains to be answered why SIV does not cause disease in its natural host. The transmission of pathogens from their natural hosts to new hosts often potentiates virulence. SIVmac, which originates from SIVsmm of sooty mangabeys, causes simian AIDS in Asian macaques (33). Similarly, it has been reported that cross-species transmission of STLV-1 from rhesus macaques to baboons induced lymphomas (13). Bovine leukemia

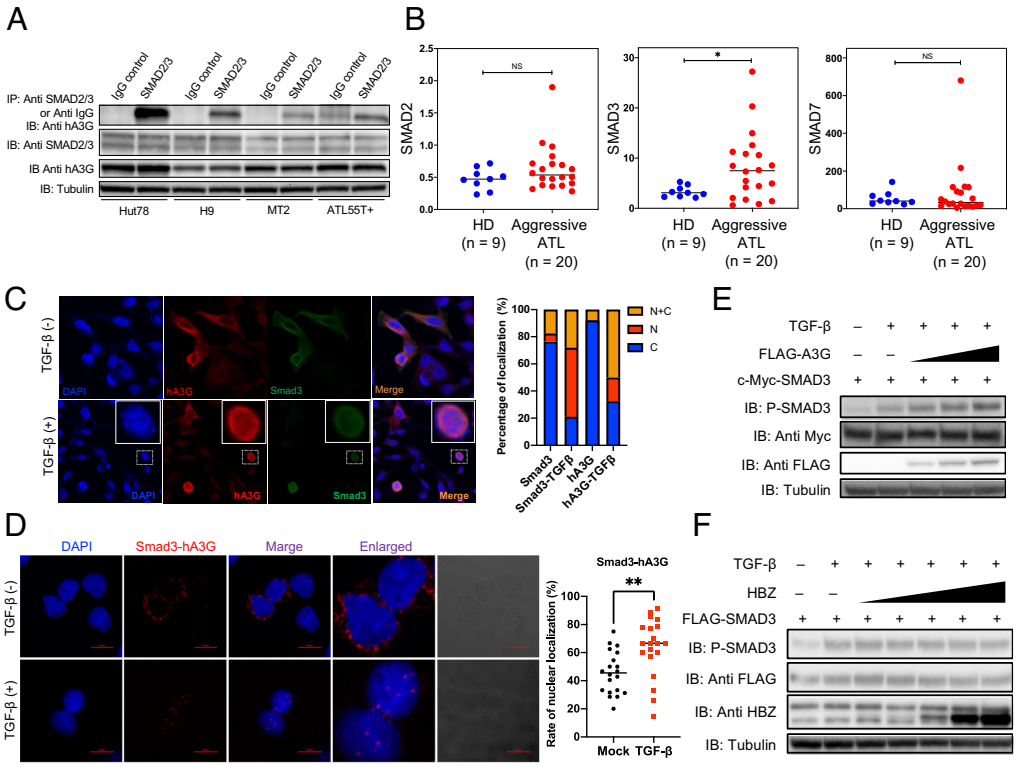

Fig. 4. Interaction between A3G and Smad proteins. (*A*) Coimmunoprecipitation experiment showing the interaction of endogenous hA3G with endogenous Smad2/3 in HTLV-1-negative T cell lines (Hut78, H9), an HTLV-1-infected T cell line (MT-2), and an ATL cell line (ATL55T+). IP, immunoprecipitation; IB, immunoblot. (*B*) Expression of Smad2, Smad3, and Smad7 in healthy donors (n = 9) and patients with aggressive ATL (n = 20) by RT-qPCR (triplicate experiments; one-way ANOVA with Tukey correction; $*P < 0.05$). (*C*) Immunofluorescence microscopy images showing the hA3G protein and Smad3 protein in the presence or absence of TGF-β (*Left*) and percentage of localization (*Right*) in transfected HeLa cells. N: nucleus, C: cytoplasm. (*D*) Complex of hA3G with Smad3 in primary ATL cells with or without TGF-β treatment, detected by the Duolink PLA (*Left*) and the rate of nuclear localization (*Right*; two-tailed unpaired Student's *t* test; $**P < 0.01$). (*E*) Immunoblot showing that hA3G expression induces the phosphorylation of Smad3 in a dose-dependent manner in transfected HepG2 cells. (*F*) Immunoblotting reveals no dose-dependent phosphorylation of Smad3 induced by HBZ expression in transfected HepG2 cells. Experiments were performed at least twice (*A* and *C*–*F*).

virus (BLV) causes B cell lymphomas in 5 to 10% of infected animals after long latency periods, which is similar to HTLV-1 (34). However, about 40% of BLV-infected sheep develop lymphomas, indicating that the pathogenicity of BLV is highly augmented by cross-species transmission (35). HTLV-1 induces ATL in approximately 5% of infected individuals (11). This study shows that maladaptation of HTLV-1 to hA3G is a mechanism of the pathogenicity of HTLV-1.

HTLV-1 originated via cross-species transmission of STLV-1 to humans that is estimated to have occurred approximately 20,000 to 50,000 y ago. The evolutionary rate of HTLV-1 is estimated to be about three logs lower than that of HIV-1 (36). Based on this estimate, the time since HTLV-1 entered into humans is equivalent to 20 to 50 y for HIV-1. This difference in evolutionary rate is caused by a difference in mode of transmission: HTLV-1 transmits primarily through cell-to-cell contact (37), whereas HIV-1 has the capacity to efficiently spread in both cell-to-cell and cell-free fashions. After transmission, HTLV-1 increases its "progeny" by proliferation of infected cells and de novo infection (38). During the carrier state, proliferation of infected cells is dominant, which means that de novo infection with reverse transcription is rare compared to other retroviruses, like HIV-1. Thus, the evolutionary rate of HTLV-1 is much lower than that of HIV-1. This study shows that HBZ can still inhibit sA3G deaminase activity, while it has not adapted to become able to inhibit hA3G. In contrast, APH-2 of HTLV-2 strongly inhibits hA3G. Cross-species transmission of HTLV-2 is thought to have occurred about 400,000 y ago (39); thus it has had roughly ten times longer than HTLV-1 to adapt to humans. Therefore, APH-2/HTLV-2 might have had enough time to evolve the ability to efficiently inhibit hA3G, whereas HTLV-1 is vulnerable to hA3G due to insufficient adaptation to humans. The difference in pathogenicity between HTLV-1 and HTLV-2 might reflect inadequate adaptation of HTLV-1 to humans. HBZ cannot suppress the deaminase activity of hA3G, but HBZ and hA3G potentiate the TGF-β/Smad pathway, leading to proliferation of ATL cells. Meanwhile, as the pathogenesis of STLV-1 has not been extensively studied, it remains to be studied how HBZ/hA3G plays a role in the leukemogenesis.

A3G functions as an antiretroviral host factor that targets ssDNA for mutation during reverse transcription (18, 40). Retroviruses have acquired a variety of mechanisms to counteract A3G (20, 41, 42). This study reveals that the antisense proteins, APH-2, SBZ, and HBZ, interact with A3G and (for the version of A3G to which they are adapted) suppress its antiretroviral function. Exactly how antisense proteins hinder the deaminase activity of A3G remains to be elucidated. Unexpectedly though, hA3G and HBZ also work together to synergistically enhance TGF-β/Smad signaling, resulting in the promotion of the proliferation of infected cells and lymphomagenesis. This does not occur for antisense protein/A3G combinations that are better adapted to one another, such as APH-2/hA3G or SBZ/sA3G (Fig. 3*D*). Thus, the lack of adaptation of HBZ to human hosts means that contrary to its typical antiviral activity, hA3G actually augments the pathogenetic effects of HBZ.

TGF-β plays important roles in different steps of oncogenesis: epithelial–mesenchymal transition, metastasis, and suppression of host immunity (43–45). However, until now it has not been reported that TGF-β positively contributes to the proliferation of cancer cells. Meanwhile, HBZ plays a central role in HTLV-1-infected cells and ATL (46). HBZ determines the immunophenotypes of infected cells and ATL cells, promotes the proliferation of infected cells, and also inhibits apoptosis (46). HBZ activates the TGF-β/Smad pathway through interaction with a coactivator, p300, and induces expression of Foxp3 (31), which converts expressing cells to become regulatory T-like cells. This study reveals that TGF-β/Smad signaling is activated by hA3G as well as HBZ and plays an important role in ATL leukemogenesis by up-regulating *BATF3/IRF4* and *MYC*, which are reported to be critical for the proliferation of ATL cells (32). Proliferation was suppressed by blockage of the TGF-β/Smad pathway in most ATL cell lines and HTLV-1-infected cell lines, although the inhibitory effect was not observed in a few cell lines.

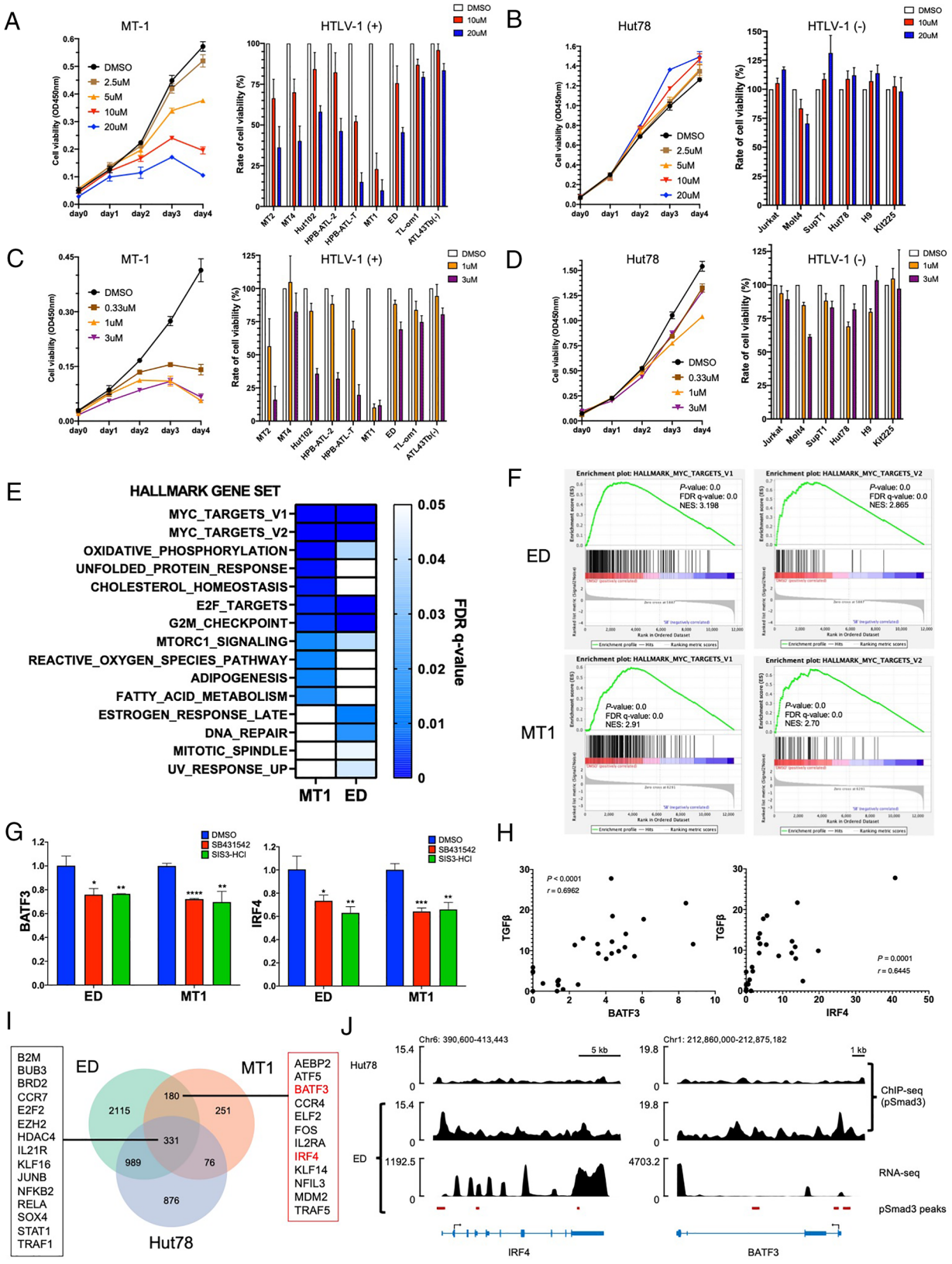

Fig. 5. Blockage of TGF-β/Smad signaling suppresses ATL cell proliferation. (*A* and *B*) Cell growth of MT-1 (*A*) Hut78 (*B*) cells treated with SB431542 (*Left*), and cell growth rates of assorted HTLV-1-infected T cell lines (n = 9) (*A*) and HTVL-1 noninfected T cell lines (n = 6) (*B*) treated with SB431542 at day 4 are shown (*Right*) (normalized mean ± SD of triplicate experiments). (*C* and *D*) Cell growth of MT-1 (*C*) Hut78 (*D*) cells treated with SIS3-HCl cell (*Left*), and cell growth rates of assorted HTLV-1-infected T cell lines (n = 9) (*C*) and HTVL-1 noninfected T cell lines (n = 6) (*D*) treated with SIS3-HCl at day 4 are shown (*Right*) (normalized mean ± SD of triplicate experiments). (*E*) Hallmark gene sets down-regulated in MT-1 and ED cells upon treatment with SB431542, analyzed by RNA-seq. (*F*) Significantly enriched gene signatures for Myc-related gene sets in SB431542 treated ED cells and MT-1 cells, determined by GSEA analysis with RNA-seq. (*G*) *BATF3* and *IRF4* expression in ED and MT-1 cells treated with SB431542 or SIS3-HCl, analyzed by RT-qPCR (one-way ANOVA with Tukey correction; *$P < 0.05$; **$P < 0.01$; ***$P < 0.001$; ****$P < 0.0001$). (*H*) Correlation of TGF-β protein with BATF3 protein or IRF4 protein in fresh ATL cells (n = 26), detected by multiplex mass-cytometry analysis (CyToF) (Pearson correlation analysis). (*I*) Venn diagram of differently expressed genes (DEG) by ChIP-seq in ED cells, MT-1 cells, and Hut78 cells. (*J*) Enrichment of phosphorylated Smad3 in *BATF3* and *IRF4* genes demonstrated by ChIP-seq analysis in an ATL cell line (ED) and a non-ATL T cell line (Hut78).

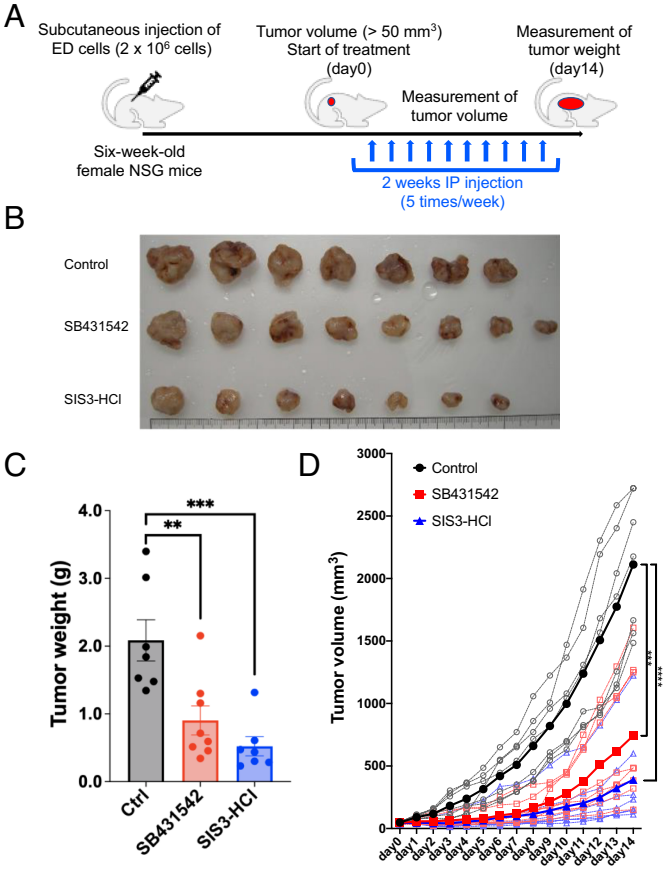

Fig. 6. In vivo effect of blockage of TGF-β/Smad signaling on ATL. (*A*) Schematic representation of the xenograft model of ATL. (*B*) ATL tumor growth in mice treated with control (n = 7), SB431542 (n = 8), or SIS3-HCl (n = 7). (*C* and *D*) ATL tumor weights (normalized mean ± SD) (*C*) and volumes (*D*) in mice treated with control (n = 7), SB431542 (n = 8), or SIS3-HCl (n = 7) are shown (one-way ANOVA with Tukey correction; $^{**}P < 0.01$; $^{***}P < 0.001$; $^{****}P < 0.0001$).

TGF-β also suppresses immune responses (43), which helps cancer cells evade host immune surveillance. In this sense, TGF-β has dual functions in ATL: growth promotion and immune evasion. Similarly, HBZ enhances production of an immunosuppressive cytokine, IL-10, that also promotes the proliferation of HBZ-expressing cells through interaction with STAT (47). Thus, HTLV-1 utilizes two immunosuppressive cytokines, TGF-β and IL-10, to promote the proliferation of infected cells. This strategy of HTLV-1 is likely associated with HTLV-1-related inflammatory diseases including HAM. In these inflammatory diseases, increases in the number of HTLV-1-infected cells are implicated in pathogenesis (48). Therefore, the growth-promoting activity of enhanced TGF-β/Smad signaling through HBZ/hA3G may play a role in the development of inflammatory diseases.

HBZ activates the TGF-β/Smad pathway through interaction with Smad3 and p300 without enhanced phosphorylation of Smad3 (*SI Appendix*, Fig. S10). Likewise, hA3G interacts with Smad3 and activates this pathway via increased phosphorylation of Smad3. HBZ and hA3G synergistically potentiate the TGF-β/Smad pathway through different mechanisms, which results in enhanced proliferation by up-regulated expression of *BATF3* and *IRF4*. This study shows that the incomplete adaptation of HTLV-1 to hA3G paradoxically enhances the pathogenicity of HTLV-1. Thus, we reveal the molecular mechanism by which inadequate adaptation of a virus to its new host is linked with its pathogenicity.

Materials and Methods

Clinical Samples. Blood samples were obtained from HTLV-1 carriers, patients with ATL, and HTLV-2-infected individuals. Peripheral blood mononuclear cells (PBMCs) were collected using Ficoll-Paque PLUS (GE Healthcare). All subjects were fully informed of the purpose and procedures of this study, and written informed consent was obtained from each subject in accordance with the Declaration of Helsinki. Use of the clinical samples in this research was approved by the Ethics Committee of Kyoto University (approval no. G204) and Kumamoto University (Genome 297).

Japanese Macaque Samples. Japanese macaques (*Macaca fuscata*) were reared in the Primate Research Institute, Kyoto University. Blood samples were obtained from the macaques for routine veterinary and microbiological examination under ketamine anesthesia with medetomidine. The animal experiment was approved by the Animal Welfare and Animal Care Committees of Kyoto University (approval numbers R11-11, R12-01, R13-01, R14-01, R15-01, B12-3, and B19-1) and was carried out in accordance with the Guidelines for Care and Use of Nonhuman Primates (Version 3) by the Animal Welfare and Animal Care Committee of KUPRI.

Statistical Analysis. All experiments were biologically and/or technically replicated at least twice. Statistical analyses were performed using Prism 8 (GraphPad Software). Statistical significances of two group comparisons were determined using the two-tailed unpaired Student's *t* test. Multiple comparisons were performed by one-way or two-way ANOVA with Tukey correction. The minimum significance level was set at $P < 0.05$. Asterisks indicate the statistical significance as follows: $^{*}P < 0.05$; $^{**}P < 0.01$; $^{***}P < 0.001$; $^{****}P < 0.0001$.

Cells. Human embryonic kidney cell lines HEK293T were purchased from the American Type Culture Collection. HEK293T, QT6, HeLa, TZM-bl, and HepG2 cells were cultured in Dulbecco's modified Eagle's medium (Nacalai Tesque) supplemented with 10% fetal bovine serum (FBS) and antibiotics. The Jurkat cell line was provided by S. Sakaguchi, Osaka University. HTLV-1 immortalized cell lines (MT-2, MT-4 and Hut102), ATL cell lines (MT-1, HPB-ATL-2, HPB-ATL-T, ATL-43Tb(-), ED, and TL-Om1), and T cell lines not infected with HTLV-1 (Jurkat, Molt4, SupT1, Hut78, and H9) were cultured in RPMI 1640 (Nacalai Tesque) with 10% FBS and antibiotics. ATL-55T(+) and Kit225 were grown in RPMI 1640 (Nacalai Tesque) with 10% FBS, recombinant human IL-2 and antibiotics. All cells were grown at 37 °C in a 5% CO_2 atmosphere.

Mice. NOD.Cg-PrkdcscidIl2rgtm1Wjl/SzJ (NSG) mice were purchased from Charles River Laboratories Japan, Inc. All animal experiments were performed in accordance with Kumamoto University Animal Care and Use Committee guidelines and were approved by the Committee.

Xenograft Experiments. Two million ED40515(-) cells, derived from a patient with ATL, were injected subcutaneously into the right flank of 6-wk-old female NSG mice. After the tumor volume became approximately 50 mm^3, mice were randomly assigned into three groups, the control group (n = 7), treatment of the SB431542 group (Selleck) (10 mg/kg, n = 8), and treatment of the SIS3-HCl (Selleck) group (5 mg/kg, n = 7), and the drugs were given by intraperitoneal injection 5 d a week for 2 wk. The subcutaneous tumor burden was measured every day with a vernier caliper. Tumor volumes (mm^3) were calculated using the following formula: 0.5× (longest length) × (width)^2. On day 14 after the beginning of treatment, mice were killed, and the tumor weights were measured. In general, animals were killed when their tumors reached 2 cm or when the mice became moribund.

Plasmids. The infectious clone of HTLV-1 (pX1MT-M) was provided by David Derse (49). The infectious clone of HTLV-2 (pH6neo) was previously described (50). The infectious clone of STLV-1 (pWK1699) was generated by cloning of the provirus from Japanese macaques. The expression plasmids pcDNA3.1-FLAG-hA3G (wild-type [WT]), -hA3G (E259Q), -hA3D (WT), and -hA3F (WT) were prepared as previously described (51). The expression plasmids pcDNA3.1-FLAG-hA3C and -hA3H were generated by cloning from a healthy donor. The expression plasmid pcDNA3.1-FLAG-sA3G was generated by cloning from Japanese macaques. Expression plasmids for deletion or chimeric mutants of A3G were created using PCR or overlapping PCR. The plasmids pcDNA-mycHis-HBZ and -APH-2 were prepared as previously described (31, 52). The plasmid pcDNA-mycHis-SBZ was generated by subcloning SBZ from pME18Sneo (12). Deletion mutants of HBZ/APH-2/SBZ were generated by PCR. The 3TP-Lux construct contains both the phorbol myristate acetate-response elements and the Smad3/4

binding sites of the PAI-1 promoter. phRL-TK was purchased from Promega. Expression plasmid for Smads was prepared as previously described (31).

In Vitro Cytosine Deaminase Activity Assay. To evaluate the cytosine deaminase activity of A3G in vitro, a fluorescence resonance energy transfer–based assay was performed as previously described (28). QT6, a quail cell line that does not have any endogenous cytosine deaminase activity (53), was transfected with an A3G-expression vector (empty, hA3G, or sA3G) or vectors expressing HBZ, APH-2, or SBZ. After 48 h, cells were resuspended in lysis buffer (0.626% NP40, 10 mM tris-acetate pH 7.4, 50 mM potassium acetate, 100 mM NaCl, 10 mM ethylenediaminetetraacetic acid (EDTA), protease inhibitor cocktail, and DTT) and incubated on ice for 30 min.

Cell lysates were centrifuged at 13,000 rpm for 20 min to remove debris. The cell supernatants were then transferred to a new prechilled tube and stored at −80 °C prior to use. Protein concentrations were determined by using BCA Protein Assay (Thermo Fisher Scientific) and confirmed by immunoblot assay. The oligonucleotides were synthesized with labeling by TAMRA and FAM fluorophores (Bex).

Before adding oligonucleotides, A3G protein was mixed with antisense protein, adjusted to a total volume of 25 μL with lysis buffer, and incubated on ice for 20 min. Then, 25 μL of buffer [20 pmoles of oligonucleotide, 10 μg RNase A and 0.04 U uracil DNA glycosylase, 100 mM Tris pH 7.4, and 20 mM EDTA buffer] was added and then incubated at 37 °C for 5 h. Next, 30 μL of 2 M Tris-acetate (pH 7.9) was added to each well, and the plate was incubated at 95 °C for 2 min and at 6 °C for 3 min with the StepOnePlus Real-Time PCR System (Applied Biosystems). To evaluate a relative change of fluorescence due to A3G activity, the endpoint fluorescence for QT6 cells transfected by FLAG empty vector was subtracted from all experimental samples for each dose. All experiments were performed three independent times.

Deep Sequencing Analysis. Genomic DNA from HTLV-1 carriers, ATL patients, HTLV-2–infected individuals, and STLV-1–infected Japanese macaques was extracted with phenol–chloroform. To amplify the whole provirus sequences of HTLV-1, HTLV-2, and STLV-1, long PCR was performed. The primers used in this study are shown in *SI Appendix*, Table S2. The libraries were prepared using the Nextera XT DNA Library Preparation Kit (Illumina), according to the manufacturer's instructions. Then deep sequencing analysis was performed with MiSeq (Illumina). Data were analyzed using the CLC Genomics Workbench version 11.0.1. Sequenced data were trimmed and mapped to the reference sequences. Variants were analyzed using the Low Frequency Variant Detection tool. Reference GenBank numbers were AB513134 for HTLV-1 Japanese subgroup, L36905 for HTLV-1 transcontinental subgroup, NC_001488 for HTLV-2a, L20734 for HTLV-2b, and MH542226 for STLV-1.

Definition of Mutations. Genomic DNA from HEK293T cells transfected with pX1MT-M was extracted, and long-PCR was performed. Deep sequencing analysis was performed and mapped to the pX1MT-M sequence. No error variants of less than 1% were observed for each nucleotide with coverage greater than 2,000. Mutations were defined as >1% variation for each nucleotide with coverage >2,000.

Validation Analysis of Mutations. Mutations detected by deep sequencing analysis were validated using HYPERMUT software (https://www.hiv.lanl.gov/content/sequence/HYPERMUT/hypermut.html).

Phylogenetic Analysis. Complete env sequences from 65 HTLV-1 ACs and the reference strains (Japanese subgroup for ATK_J02029, YS_U119949, and AB513134; transcontinental subgroup for TSP1_M86840 and BOI_L36905) were analyzed using the k-mer-based tree construction method in the CLC Genomics Workbench version 11.0.1. The circular cladogram was generated with the neighbor-joining method.

In Vitro De Novo Infection Assay. HEK293T cells were seeded on a 6-well plate. After 24 h, the cells were cotransfected with HTLV-1, HTLV-2, or STLV-1 infectious clones in the presence or absence of a vector expressing an hA3 family gene or sA3G. After 48 h, the transfected cells were seeded on a 96-well plate and cocultured with CFSE-labeled Jurkat cells. After 48 h, Jurkat cells were collected by cell sorting (AriaIII). Then, genomic DNA was extracted and the provirus sequences were analyzed.

Viral Infectivity Assays. HEK293T cells were seeded on a 6-well plate. After 24 h, the cells were cotransfected with pNL4.3/ΔVif/ΔEnv, vectors expressing VSV-G, the indicated viral genes, and/or A3G. At 48 h after transfection, supernatants were collected and filtered with a 0.45 μm membrane. Quantification of virus particles was performed using an HIV-1 p24 ELISA Kit (ZeptoMetrix). TZM-bl cells were plated at 5×10^3 into a 96-well plate and infected with 1 ng p24 of virus particles. After 48-h incubation, cell lysates were collected using 100 μL of Glo Lysis Buffer (Promega), and luciferase activity was measured in 20 μL of lysate using the Luciferase Assay System (Promega) on a Lumat LB9501 (Berthold). The data represent the mean ± SD of three independent experiments.

Luciferase Assay. The 3TP-Lux luciferase assay was performed as previously described with minor modifications (31). Briefly, HepG2 cells (1×10^5 per well) were seeded into a 24-well plate. After 24 h, cells were transfected with the indicated plasmid. Total plasmid DNA levels were kept constant with empty vector. At 24 h after transfection, cells were treated with or without recombinant human TGF-β1 (Wako, 10 ng/mL). After 24 h, luciferase activity was measured using the Dual-Glo Luciferase Assay System (Promega) according to the manufacturer's instructions. All experiments were performed in triplicate.

Coimmunoprecipitation Experiments. HEK293T cells were seeded into a 6-well plate, incubated for 24 h, and then transfected with the indicated plasmids. After 48 h, cells were lysed in radio-immunoprecipitation assay (RIPA) buffer with protease inhibitor for 30 min on ice. The lysates were immunoprecipitated with antibody-conjugated SureBeads Protein G Magnetic Beads (BioRad). For immunoprecipitation, the following antibodies were used: mouse anti-FLAG (M2) antibody (Sigma-Aldrich) and rabbit anti-His antibody (MBL).

For endogenous immunoprecipitation experiments, Hut78, H9, MT2, or ATL55T (+) cells were lysed in RIPA buffer with protease inhibitor for 30 min on ice. Normal rabbit IgG (Wako) was used as a control. Rabbit anti-Smad2/Smad3 antibody (GeneTex, GTX111123) and rabbit anti-Smad7 antibody (Novus Biologicals, NBP2-24710) were used for Smad2/3 and Smad7 immunoprecipitation, respectively. Rabbit anti-HBZ polyclonal antibody was generated by immunizing with HBZ-peptides (CRGPPGEKAPPRGETH and QERRERKWRQGAEKC) (Medical Biological Laboratories).

Immunoblotting. For immunoblotting, the following antibodies were used: mouse anti-c-Myc (9E10) antibody (Sigma-Aldrich); rabbit anti-FLAG, mouse anti-FLAG (M2), and mouse anti-α-Tubulin (DM1A) antibodies (Sigma-Aldrich); rabbit anti-c-Myc antibody, rabbit anti-His antibody, rabbit anti-V5 antibody, rabbit anti-HA antibody, and rabbit anti-VSVG antibody (MBL); mouse anti-HTLV-I p19 antibody (clone 45/6.11.1.3) (ZeptoMetrix Corporation); rabbit anti-phospho Smad3 (C25A9) and rabbit anti-phospho-Smad2 (138D4) antibodies (Cell Signaling Technology); rabbit anti-Smad2/Smad3 antibody (GeneTex); rabbit anti-Smad7 antibody (Novus Biologicals); anti-mouse IgG-HRP (Thermo Fisher Scientific); and anti-rabbit IgG-HRP (GE Healthcare Life Sciences). Polyclonal rabbit anti-Human APOBEC3G, C-terminal (10201) was obtained from the NIH HIV Reagent Program, Division of AIDS, NIAID, NIH. Immunoblot data were obtained using ImageQuant LAS 4000 mini (GE Healthcare) or the ChemiDoc imaging system (Bio-Rad).

MG132 Treatment. To evaluate the degradation of A3G protein, we treated HBZ/APH-2/SBZ expressing HEK293T cells with the proteasome inhibitor MG132 (Cell Signaling Technology, 10 μM). After 24 h, cells were lysed in RIPA buffer, and their proteins were fractionated by sodium dodecyl sulfate/polyacrylamide gel electrophoresis (SDS/PAGE) and transferred to immunoblot membranes.

Immunofluorescence Analysis. HeLa cells and HepG2 cells were seeded on chamber slides (Matsunami Glass). After 24 h, these cells were transfected with pcDNA-myc-Smad3 and pcDNA-FLAG-hA3G using TransIT-LT1 (Mirus). At 48 h after transfection, cells were treated with or without recombinant human TGF-β1 (Wako, 10 ng/mL) for 1 h and then washed with phosphate-buffered saline (PBS), fixed with 4% paraformaldehyde for 15 min, permeabilized with 0.2% Triton X-100 for 15 min, and blocked with incubation in 5% donkey serum (Jackson ImmunoResearch). For immunostaining, cells were incubated with mouse anti-Myc (Sigma-Aldrich) and rabbit anti-FLAG (Sigma-Aldrich) antibodies, followed by incubation with Alexa Fluor 488–conjugated donkey anti-mouse IgG (Invitrogen) and Alexa Fluor 594–conjugated donkey anti-rabbit IgG antibodies (Invitrogen), respectively. The stained cells were mounted with ProLong Gold Antifade Reagent with DAPI (Molecular Probes), imaged using a C2 confocal microscope (Nikon), and analyzed with ImageJ.

Duolink PLA. PBMCs from ATL patients were washed and centrifuged onto APS-coated glass slides (Matsunami Glass) by Cytospin (Shandon). Cells were then fixed with 4% paraformaldehyde, permeabilized, and blocked with Duolink Blocking Solution. After that, cells were stained with mouse anti-HBZ antibody (1A10, generated by immunizing C57BL/6 mice with keyhole limpet hemocyanin [KLH]– conjugated HBZ peptide 97–133 [CKQIAEYLKRKEEEKARRRRRAEKKAADVARRKQEEQE]) or mouse anti-Smad3 (7F3, Sigma-Aldrich) and rabbit anti-human APOBEC3G

antibody (D9C6Z, Cell Signaling Technology), which were diluted in Duolink Antibody Diluent, followed by incubation with Duolink In Situ PLA Probe Anti-Mouse PLUS and Duolink In Situ PLA Probe Anti-Rabbit MINUS. Next, cells were incubated with Duolink 5× Ligation Buffer and Duolink Polymerase (10 u/μL), followed by incubation with Duolink Amplification Red and Duolink Ligase (1 U μL). The stained cells were mounted with Duolink®In Situ Mounting Medium with DAPI. The cells were imaged using a C2 confocal microscope (Nikon) and analyzed with ImageJ.

Viral Incorporation Assay. HEK293T cells were seeded on a 6-well plate. After 24 h, the cells were cotransfected with infectious clones (pX1MT-M/ΔEnv, or pH6neo/ΔEnv, and pWK1699/ΔEnv) and vectors expressing VSV-G, and/or A3G (hA3G or sA3G). At 48 h after transfection, supernatants were collected and filtered with a 0.45 μm membrane. For the endogenous viral incorporation experiment, the supernatants of MT2 cells were collected and filtered with a 0.45 μm membrane. Virus particles were concentrated by ultracentrifugation using Beckman Optima XPN−100 at 25,000 rpm for 2 h at 4 °C. Virus particles and cells were lysed separately in RIPA buffer, and their proteins were fractionated by SDS/PAGE and transferred to immunoblot membranes.

shRNA Knockdown and Cell Sorting. Knockdown of hA3G was performed by using the GIPZ Lentiviral Human APOBEC3G shRNA and its control (RHS4531-EG60489 glycerol set, Dharmacon) according to the manufacturer's instructions. VP were produced in HEK293T cells and purified by ultracentrifugation (25,000g for 120 min at 4 °C). Target cells were infected with lentivirus for 48 h. Stable transfectants were selected in puromycin (10 μg/mL). For RNA-seq analysis, GFP-positive cells were collected by cell sorting (AriaIII) after puromycin selection.

RNA Extraction and RNA-seq. RNA was extracted using the ReliaPrep RNA Miniprep System (Promega). Library preparation and high-throughput sequencing were performed at Macrogen using the TruSeq RNA Sample Prep Kit v2 and HiSeq 2000 (Illumina). RNA-seq data were mapped to the h38 using STAR (54). Differently expressed genes were analyzed using RSEM (55) and edgeR (56).

Quantitative RT-PCR. $CD4^+$ T cells were isolated from PBMCs of ATL patients and healthy donors using selection beads (BD IMag™). Total RNA was extracted using Trizol Reagent (Invitrogen) or ReliaPrep RNA Miniprep System (Promega). cDNAs were synthesized by reverse transcription using Superscript IV Reverse Transcriptase (Thermo Fisher Scientific). Quantitative real-time PCR was performed using real-time PCR using FastStart Universal SYBR Green Master (Roche) and the StepOnePlus Real-Time PCR System (Applied Biosystems). Primers used in this study are shown in *SI Appendix*, Table S2.

ChIP Sequencing. ChIP DNAs were obtained from ED cells, MT-1 cells, and Hut78 cells with rabbit anti-phospho Smad3 antibody (C25A9, Cell Signaling Technology) according to the SimpleChIP Enzymatic Chromatin IP Kit protocol (Cell Signaling Technology). We used the TruSeq ChIP Library Preparation Kit (Illumina); subsequently, libraries were sequenced on the Illumina NovaSeq6000 platform with a standard 150-bp paired-end read protocol. Sequenced fastq files were qualified and trimmed with TrimGalore. We aligned them to the human genome (hg19) using Bowtie2 with the "--very-sensitive" option (57). Mapped reads with "XS" or "MT" tags were excluded. We also deleted PCR duplicates by Picard (MarkDuplicates) and the ENCODE Blacklist genome regions (58). To detect significant peaks in comparison to input DNA, we used MACS2 (59) with a cutoff p-value less than 1e-5. Subsequent analyses for visualization of ChIP-seq were done using samtools (60), deeptools (61), and SparK (62).

CyTOF. Meta-tagged monoclonal antibodies were purchased and labeled using the Maxpar X8 Antibody Labeling Kit (Fluidigm) according to the manufacturer's recommended protocol. These antibodies were titrated and diluted to 0.5 mg/mL in Antibody Stabilizer (CANDOR Bioscience) for long-term storage at 4 °C. PBMCs from ATL patients were stained in PBS supplemented with 0.2 μM Cisplatin Cell-ID (Fluidigm). After washing and blocking, cells were incubated with antibodies targeting cell surface markers. After washing, cells were fixed and permeabilized on ice using eBioscience FoxP3 fix/perm (Thermo Fisher Scientific). Fixed/permeabilized cells were washed and incubated with all antibodies targeting intracellular antigens. After staining, cells were washed and incubated with Ir DNA intercalator (Fluidigm). The next day, cells were washed and resuspended in water containing EQ Four Element Calibration Beads (Fluidigm). Samples were acquired on a Helios CyTOF System (Fluidigm). All gating and extraction of median expression levels was analyzed using Cytobank.

Cell Proliferation Assay. Cells were seeded into 96-well plates and treated with DMSO, SB431542 (Selleck) or SIS3-HCl (Selleck) at the indicated concentration. Cell growth was assessed by using a Cell Counting Kit-8 (DOJINDO LABORATORIES) according to the manufacturer's instructions.

Data, Materials, and Software Availability. Data of deep sequencing, RNA-seq, and ChIP-seq in this study have been deposited at the DNA Data Bank of Japan (DDBJ) (accession number DRA017056) (63).

ACKNOWLEDGMENTS. We thank Chiho Onishi and Miho Matsumoto for technical support, Kazuya Shimura and Guangyong Ma for technical advice, and Linda Kingsbury for proofreading. AMED, Project for Cancer Research And Therapeutic Evolution 20cm0106306h0005 (J.-i.Y. and M.M.) AMED, Research Program on Emerging and Re-emerging Infectious Diseases (20fk0108088h0002) (J.-i.Y. and M.M.) AMED, Science and Technology Platform Program for Advanced Biological Medicine (21am0401003h0003) (J.-i.Y.) JSPS KAKENHI (19H03689 to M.M.) JSPS KAKENHI (20H03514 to J.-i.Y.) JSPS KAKENHI (23K15303 to T.S.) NIH grant CA100730 (P.L.G.) NIH grant CA234228 (R.S.H.) JSPS Leading Initiative for Excellent Young Researchers (T.I.) JSPS Core-to-Core Program A, Advanced Research Networks (J.-i.Y. and M.M.) Nippon Shinyaku Research Grant (T.S.) Friends of Leukemia Research Fund (T.S.) Okukubo Memorial Fund for Medical Research in Kumamoto University (T.S.) Center for Metabolic Regulation of Healthy Aging (T.S.).

Author affiliations: [a]Department of Hematology, Rheumatology and Infectious Diseases, Faculty of Life Sciences, Kumamoto University, Kumamoto 860-8556, Japan; [b]Laboratory of Virus Control, Institute for Life and Medical Sciences, Kyoto University, Kyoto 606-8507, Japan; [c]Division of Systems Virology, Institute of Medical Science, The University of Tokyo, Tokyo 108-8639, Japan; [d]Core Research for Evolutional Science and Technology (CREST), Japan Science and Technology Agency, Saitama 332-0012, Japan; [e]Laboratory of Systems Virology, Institute for Life and Medical Sciences, Kyoto University, Kyoto 606-8507, Japan; [f]Department of Laboratory Medicine, University of California, San Francisco 94158; [g]Department of Epidemiology/Biostatistics, University of California, San Francisco; [h]Vitalant Research Institute, San Francisco 94105; [i]Department of Hematology, Osaka General Hospital of West Japan Railway Company, Osaka 545-0053, Japan; [j]Center for the Evolutionary Origins of Human Behavior, Kyoto University, Inuyama, Aichi 484-8506, Japan; [k]Division of Molecular Virology and Genetics, Joint Research Center for Human Retrovirus infection, Kumamoto University, Kumamoto 860-0811, Japan; [l]Department of Biochemistry and Structural Biology, University of Texas Health San Antonio, San Antonio, TX 78229; [m]HHMI, University of Texas Health San Antonio, San Antonio, TX 78229; [n]Center for Retrovirus Research, Department of Veterinary Biosciences, The Ohio State University, Columbus, OH 43210; and [o]Department of Veterinary Biosciences, The Ohio State University, Columbus, OH

1. B. J. Poiesz *et al.*, Detection and isolation of type C retrovirus particles from fresh and cultured lymphocytes of a patient with cutaneous T-cell lymphoma. *Proc. Natl. Acad. Sci. U.S.A.* **77**, 7415–7419 (1980).
2. V. S. Kalyanaraman *et al.*, A new subtype of human T-cell leukemia virus (HTLV-II) associated with a T-cell variant of hairy cell leukemia. *Science* **218**, 571–573 (1982).
3. F. Barre-Sinoussi *et al.*, Isolation of a T-lymphotropic retrovirus from a patient at risk for acquired immune deficiency syndrome (AIDS). *Science* **220**, 868–871 (1983).
4. F. Barin *et al.*, Serological evidence for virus related to simian T-lymphotropic retrovirus III in residents of west Africa. *Lancet* **2**, 1387–1389 (1985).
5. P. J. Kanki *et al.*, New human T-lymphotropic retrovirus related to simian T-lymphotropic virus type III (STLV-IIIAGM). *Science* **232**, 238–243 (1986).
6. F. Clavel *et al.*, Isolation of a new human retrovirus from West African patients with AIDS. *Science* **233**, 343–346 (1986).
7. G. Feuer, P. L. Green, Comparative biology of human T-cell lymphotropic virus type 1 (HTLV-1) and HTLV-2. *Oncogene* **24**, 5996–6004 (2005).
8. A. M. Vandamme, M. Salemi, J. Desmyter, The simian origins of the pathogenic human T-cell lymphotropic virus type I. *Trends Microbiol.* **6**, 477–483 (1998).
9. S. Van Dooren, M. Salemi, A. M. Vandamme, Dating the origin of the African human T-cell lymphotropic virus type-i (HTLV-I) subtypes. *Mol. Biol. Evol.* **18**, 661–671 (2001).
10. P. V. Afonso, O. Cassar, A. Gessain, Molecular epidemiology, genetic variability and evolution of HTLV-1 with special emphasis on African genotypes. *Retrovirology* **16**, 39 (2019).
11. M. Matsuoka, K. T. Jeang, Human T-cell leukaemia virus type 1 (HTLV-1) infectivity and cellular transformation. *Nat. Rev.* **7**, 270–280 (2007).
12. M. Miura *et al.*, Characterization of simian T-cell leukemia virus type 1 in naturally infected Japanese macaques as a model of HTLV-1 infection. *Retrovirology* **10**, 118 (2013).
13. A. Voevodin, E. Samilchuk, H. Schatzl, E. Boeri, G. Franchini, Interspecies transmission of macaque simian T-cell leukemia/lymphoma virus type 1 in baboons resulted in an outbreak of malignant lymphoma. *J. Virol.* **70**, 1633–1639 (1996).
14. A. Chahroudi, S. E. Bosinger, T. H. Vanderford, M. Paiardini, G. Silvestri, Natural SIV hosts: Showing AIDS the door. *Science* **335**, 1188–1193 (2012).
15. C. Apetrei *et al.*, Molecular epidemiology of simian immunodeficiency virus SIVsm in U.S. primate centers unravels the origin of SIVmac and SIVstm. *J. Virol.* **79**, 8991–9005 (2005).
16. P. M. Sharp, B. H. Hahn, Origins of HIV and the AIDS pandemic. *Cold Spring Harb Perspect Med.* **1**, a006841 (2011).

17. D. Sauter, F. Kirchhoff, Key viral adaptations preceding the AIDS pandemic. *Cell Host Microbe* **25**, 27–38 (2019).
18. R. S. Harris, M. T. Liddament, Retroviral restriction by APOBEC proteins. *Nat. Rev. Immunol.* **4**, 868–877 (2004).
19. M. H. Malim, P. D. Bieniasz, HIV restriction factors and mechanisms of evasion. *Cold Spring Harb. Perspect. Med.* **2**, a006940 (2012).
20. A. M. Sheehy, N. C. Gaddis, J. D. Choi, M. H. Malim, Isolation of a human gene that inhibits HIV-1 infection and is suppressed by the viral Vif protein. *Nature* **418**, 646–650 (2002).
21. R. S. Harris *et al.*, DNA deamination mediates innate immunity to retroviral infection. *Cell* **113**, 803–809 (2003).
22. D. Derse, S. A. Hill, G. Princler, P. Lloyd, G. Heidecker, Resistance of human T cell leukemia virus type 1 to APOBEC3G restriction is mediated by elements in nucleocapsid. *Proc. Natl. Acad. Sci. U.S.A.* **104**, 2915–2920 (2007).
23. J. Fan *et al.*, APOBEC3G generates nonsense mutations in human T-cell leukemia virus type 1 proviral genomes in vivo. *J. Virol.* **84**, 7278–7287 (2010).
24. F. Poulain, N. Lejeune, K. Willemart, N. A. Gillet, Footprint of the host restriction factors APOBEC3 on the genome of human viruses. *PLoS Pathog.* **16**, e1008718 (2020).
25. Q. Yu *et al.*, Single-strand specificity of APOBEC3G accounts for minus-strand deamination of the HIV genome. *Nat. Struct. Mol. Biol.* **11**, 435–442 (2004).
26. G. Gaudray *et al.*, The complementary strand of the human T-cell leukemia virus type 1 RNA genome encodes a bZIP transcription factor that down-regulates viral transcription. *J. Virol.* **76**, 12813–12822 (2002).
27. M. Halin *et al.*, Human T-cell leukemia virus type 2 produces a spliced antisense transcript encoding a protein that lacks a classic bZIP domain but still inhibits Tax2-mediated transcription. *Blood* **114**, 2427–2438 (2009).
28. C. M. Holtz, H. A. Sadler, L. M. Mansky, APOBEC3G cytosine deamination hotspots are defined by both sequence context and single-stranded DNA secondary structure. *Nucleic Acids Res.* **41**, 6139–6148 (2013).
29. S. Fredriksson *et al.*, Protein detection using proximity-dependent DNA ligation assays. *Nat. Biotechnol.* **20**, 473–477 (2002).
30. K. Kataoka *et al.*, Integrated molecular analysis of adult T cell leukemia/lymphoma. *Nat. Genet.* **47**, 1304–1315 (2015).
31. T. Zhao *et al.*, HTLV-1 bZIP factor enhances TGF-{beta} signaling through p300 coactivator. *Blood* **118**, 1865–1876 (2011).
32. M. Nakagawa *et al.*, Targeting the HTLV-I-regulated BATF3/IRF4 transcriptional network in adult T cell leukemia/lymphoma. *Cancer Cell* **34**, 286–297.e10 (2018).
33. N. L. Letvin *et al.*, Induction of AIDS-like disease in macaque monkeys with T-cell tropic retrovirus STLV-III. *Science* **230**, 71–73 (1985).
34. A. Abdala *et al.*, BLV: Lessons on vaccine development. *Retrovirology* **16**, 26 (2019).
35. S. Djilali, A. L. Parodi, The BLV-induced leukemia–lymphosarcoma complex in sheep. *Vet. Immunol. Immunopathol.* **22**, 233–244 (1989).
36. P. Lemey, S. Van Dooren, A. M. Vandamme, Evolutionary dynamics of human retroviruses investigated through full-genome scanning. *Mol. Biol. Evol.* **22**, 942–951 (2005).
37. T. Igakura *et al.*, Spread of HTLV-I between lymphocytes by virus-induced polarization of the cytoskeleton. *Science* **299**, 1713–1716 (2003).
38. C. R. M. Bangham, M. Matsuoka, Human T-cell leukaemia virus type 1: Parasitism and pathogenesis. *Philos Trans. R Soc. Lond. B Biol. Sci.* **372**, 20160272 (2017).
39. A. M. Vandamme, U. Bertazzoni, M. Salemi, Evolutionary strategies of human T-cell lymphotropic virus type II. *Gene* **261**, 171–180 (2000).
40. M. H. Malim, APOBEC proteins and intrinsic resistance to HIV-1 infection. *Philos. Trans. R Soc. Lond. B Biol. Sci.* **364**, 675–687 (2009).
41. M. Lochelt *et al.*, The antiretroviral activity of APOBEC3 is inhibited by the foamy virus accessory Bet protein. *Proc. Natl. Acad. Sci. U.S.A.* **102**, 7982–7987 (2005).
42. A. A. Jaguva Vasudevan *et al.*, Prototype foamy virus Bet impairs the dimerization and cytosolic solubility of human APOBEC3G. *J. Virol.* **87**, 9030–9040 (2013).
43. M. L. Chen *et al.*, Regulatory T cells suppress tumor-specific CD8 T cell cytotoxicity through TGF-beta signals in vivo. *Proc. Natl. Acad. Sci. U.S.A.* **102**, 419–424 (2005).
44. H. L. Moses, A. B. Roberts, R. Derynck, The discovery and early days of TGF-beta: A historical perspective. *Cold Spring Harb. Perspect. Biol.* **8**, a021865 (2016).
45. H. W. Yeh, S. S. Lee, C. Y. Chang, Y. D. Lang, Y. S. Jou, A new switch for TGFbeta in cancer. *Cancer Res.* **79**, 3797–3805 (2019).
46. M. Matsuoka, J. M. Mesnard, HTLV-1 bZIP factor: The key viral gene for pathogenesis. *Retrovirology* **17**, 2 (2020).
47. Y. Higuchi *et al.*, HTLV-1 induces T cell malignancy and inflammation by viral antisense factor-mediated modulation of the cytokine signaling. *Proc. Natl. Acad. Sci. U.S.A.* **117**, 13740–13749 (2020).
48. M. Yoshida *et al.*, Increased replication of HTLV-I in HTLV-I-associated myelopathy. *Ann. Neurol.* **26**, 331–335 (1989).
49. M. S. Mitchell *et al.*, Phenotypic and genotypic comparisons of human T-cell leukemia virus type 1 reverse transcriptases from infected T-cell lines and patient samples. *J. Virol.* **81**, 4422–4428 (2007).
50. M. Anderson, P. L. Green, Growth and manipulation of a human T-cell leukemia virus type-2 full-length molecular clone. *Methods Mol. Biol.* **304**, 409–421 (2005).
51. T. Kobayashi *et al.*, Quantification of deaminase activity-dependent and -independent restriction of HIV-1 replication mediated by APOBEC3F and APOBEC3G through experimental-mathematical investigation. *J. Virol.* **88**, 5881–5887 (2014).
52. E. Douceron *et al.*, HTLV-2 APH-2 expression is correlated with proviral load but APH-2 does not promote lymphocytosis. *J. Infect Dis.* **205**, 82–86 (2012).
53. M. Henry *et al.*, Genetic editing of HBV DNA by monodomain human APOBEC3 cytidine deaminases and the recombinant nature of APOBEC3G. *PLoS One* **4**, e4277 (2009).
54. A. Dobin *et al.*, STAR: Ultrafast universal RNA-seq aligner. *Bioinformatics* **29**, 15–21 (2013).
55. B. Li, C. N. Dewey, RSEM: Accurate transcript quantification from RNA-Seq data with or without a reference genome. *BMV Bioinform.* **12**, 323 (2011).
56. M. D. Robinson, D. J. McCarthy, G. K. Smyth, edgeR: A Bioconductor package for differential expression analysis of digital gene expression data. *Bioinformatics* **26**, 139–140 (2010).
57. B. Langmead, S. L. Salzberg, Fast gapped-read alignment with Bowtie 2. *Nat. Methods* **9**, 357–359 (2012).
58. H. M. Amemiya, A. Kundaje, A. P. Boyle, The ENCODE Blacklist: Identification of Problematic Regions of the Genome. *Sci. Rep.* **9**, 9354 (2019).
59. Y. Zhang *et al.*, Model-based analysis of ChIP-Seq (MACS). *Genome Biol.* **9**, R137 (2008).
60. P. Danecek *et al.*, Twelve years of SAMtools and BCFtools. *Gigascience* **10**, giab008 (2021).
61. F. Ramirez *et al.*, deepTools2: A next generation web server for deep-sequencing data analysis. *Nucleic Acids Res.* **44**, W160–W165 (2016).
62. S. Kurtenbach, J. William Harbour, SparK: A publication-quality NGS visualization tool. bioRxiv [Preprint] (2019). https://doi.org/10.1101/845529 (Accessed 11 October 2021).
63. T. Shichijo *et al.*, Data from "Vulnerability to APOBEC3G linked to the pathogenicity of deltaretroviruses" DDBJ. https://ddbj.nig.ac.jp/public/ddbj_database/dra/fastq/DRA017/DRA017056/. Deposited 1 January 2024.